small
NANO MICRO



# Ag@Ni Core–Shell Nanowire Network for Robust Transparent Electrodes Against Oxidation and Sulfurization

*Hyeonjin Eom, Jaemin Lee, Aekachan Pichitpajongkit, Morteza Amjadi, Jun-Ho Jeong, Eungsug Lee, Jung-Yong Lee, and Inkyu Park**

***S**ilver nanowire (Ag NW) based transparent electrodes are inherently unstable to moist and chemically reactive environment. A remarkable stability improvement of the Ag NW network film against oxidizing and sulfurizing environment by local electrodeposition of Ni along Ag NWs is reported. The optical transmittance and electrical resistance of the Ni deposited Ag NW network film can be easily controlled by adjusting the morphology and thickness of the Ni shell layer. The electrical conductivity of the Ag NW network film is increased by the Ni coating via welding between Ag NWs as well as additional conductive area for the electron transport by electrodeposited Ni layer. Moreover, the chemical resistance of Ag NWs against oxidation and sulfurization can be dramatically enhanced by the Ni shell layer electrodeposited along the Ag NWs, which provides the physical barrier against chemical reaction and diffusion as well as the cathodic protection from galvanic corrosion.*

H. Eom, A. Pichitpajongkit, M. Amjadi, Prof. I. Park
Department of Mechanical Engineering
Korea Advanced Institute of Science
and Technology (KAIST)
291 Daehak-ro, Yuseong-gu
Daejeon 305–701, Republic of Korea
E-mail: inkyu@kaist.ac.kr

H. Eom, J.-H. Jeong, E. Lee
Department of Nano Manufacturing Technology
Korea Institute of Machinery & Materials (KIMM)
156 Gajeongbuk-ro, Yuseong-gu
Daejeon 305–343, Republic of Korea

J. Lee, M. Amjadi, J.-Y. Lee, Prof. I. Park
KI for the NanoCentury (KINC)
Korea Advanced Institute of Science and Technology (KAIST)
291 Daehak-ro, Yuseong-gu,
Daejeon 305–701, Republic of Korea

J. Lee, J.-Y. Lee
Graduate School of Energy
Environment, Water, and Sustainability(EEWS)
Korea Advanced Institute of Science and Technology (KAIST)
291 Daehak-ro, Yuseong-gu
Daejeon 305–701, Republic of Korea

DOI: 10.1002/smll.201400992

## 1. Introduction

Transparent conductive electrodes (TCEs) have been investigated for numerous applications including mobile display, photovoltaic energy generation, and liquid crystal display applications.[1–3] Indium tin oxide (ITO) is the most widely used material for transparent electrodes due to its high electrical conductivity and transparency in the visible range.[4] However, ITO is not suitable for flexible devices due to its poor mechanical flexibility and brittleness. The mechanical robustness of bare ITO films could be increased by the formation of multiple ITO-polymer composite layers.[5] Nevertheless, multi-layered ITO film was mechanically and electrically broken under the strain of $\varepsilon = 0.017$, which is lower than the requirement for flexible displays.[6] As alternatives to the ITO-polymer composite, solution-processible TCEs such as carbon nanotubes, graphene and metal mesh films have been intensively studied due to their superior mechanical characteristics as compared to the oxide based TCEs.[7–9]

Recently, silver nanowire (Ag NW) network structure has been studied as a promising alternative transparent electrode with several advantages such as high transparency,

good electrical conductivity, and mechanical flexibility.[10] The synthesis of Ag NWs by the polyol reaction[11–13] is very simple and high throughput for the large scale production of Ag NWs.[14] The transparent Ag NW network film can be obtained by spin-coating,[15] spray coating[16] and bar coating processes[17] due to facile formation of stable liquid phase suspension of NWs.

Despite the abovementioned advantages of Ag NWs, they cannot be used for a long term period due to their chemical instability. The electrical conductivity of Ag NWs can be easily degraded by the chemical instabilities such as oxidation and sulfurization.[18,19] For example, the exposed Ag NW network film under electrical current flow can be easilyoxidized and sulfurized by oxygen and sulfur from the air.[18] The Ag:Mg cathode of organic light emitting devices (OLED) shows the nonemissive spots at Ag:Mg cathode-organic interface owing to the gas evolution from the galvanic corrosion of the Mg/Ag couple.[20] Even if the Ag NW film is embedded within the device or protected by the polymer passivation layer, it can still be attacked though small voids or cracks.[21] Moreover, the polymer-coated Ag NW network films have a possibility to react with sulfur-containing gases since many polymers are permeable to gaseous molecules.[22] The chemical stability of the metal NWs has been recently studied for the improvement of their durability as conductive metal electrodes. For example, the AgNW network film protected by graphene oxide (GO) sheets shows better chemical stability in the air.[23] Also, Ag NW network film buried into the surface of the polymer substrate exhibited better sulfurization-resistivity than the conventional Ag NW network films that are entirely exposed to the ambient environment.[24] It took 1 minute for the buried AgNW network film to be completely nonconductive whereas only 3 s were required to completely disconnect the fully exposed Ag NW network under sulfurization condition (5 wt% $Na_2S$ solution).[24] The cupronickel (CuNi) NW network was utilized as an alternative material for transparent electrodes and showed good anti-oxidation property due to the anti-corrosion characteristics of Ni alloy in the moist condition.[25] However, the CuNi NW network provides higher electrical resistivity ($\rho = 1.33 \times 10^{-7}$–$2.34 \times 10^{-7}$ Ω m) than those of both Ag and Cu NW networks ($\rho_{Ag\ NW} = 1.29 \times 10^{-7}$ Ω m[26] and $\rho_{Cu\ NW} = 7.51 \times 10^{-8}$ Ω m.[25]

Herein, we introduce a novel method to improve the chemical resistance of the Ag NW network film based electrode by forming the Ni protective shell on the surface of the Ag NWs without degradation of their electrical conductivity. The Ni coated Ag NW network film is prepared by the local electrodeposition, and its superior anti-oxidation and anti-sulfurization characteristics are investigated in this work. **Figure 1**a shows the mechanisms of the anti-oxidation and anti-sulfurization of Ni coated Ag NW network film under oxygen species ($O_2$ and $OH^-$) and sulfur(S)-containing environments. As shown in the inset of Figure 1a, the Ni shell layer deposited on Ag NWs acts as an electron-donor to Ag NWs as well as a physical barrier against the reaction or diffusion of $O_2$ and $OH^-$ so that the oxidation of Ag NWs in oxygen environment is prevented. In the case of the sulfur-containing environment, the Ni shell layer on the exposed area of the Ag NW network film protects the Ag NW network film from sulfurization by similar mechanisms.

Ag NWs were synthesized by the polyol method.[14] The synthesis processes are explained in the experimental section with details. Figure 1b–f shows the schematic of the Ni coated Ag NW network film on the flexible polymer substrate (polydimethylsiloxane (PDMS) film in this study). First, the Ag NW network film is formed on the donor substrate (polyimide (PI) film in this study) by spray coating process (Figure 1b). Then, the Ag NW network film is pressed by a PDMS block to attach Ag NWs firmly onto the PI substrate and to strengthen the bonding between Ag NWs so that the soaking of the liquid PDMS into the gap between Ag NWs can be prevented. Then, the liquid PDMS is poured on the Ag NW network film and cured in a convection oven at 100 °C for 4 h, and the Ag NW network film partially embedded on the PDMS layer is peeled off from the PI film (Figure 1c,d). Partial embedding formed the robust Ag NW-PDMS composite thin film on the PDMS layer and prevented the Ag NWs from being detached during the electrodeposition process. Finally, the Ni layer is electrodeposited on the exposed surface of the Ag NW network film (see Figure 1e,f) by using a 3-eletrode system in a Ni electrodeposition bath for various time periods. (Detail of electrodeposition process is explained in the Experimetal Section.) The thickness of the Ni layer can be controlled by the electrodeposition period (Figure 1f).

## 2. Results and Discussion

**Figure 2**a shows the surface morphologies of the Ag NW network film partially buried on the surface of PDMS substrate. The average diameter and length of Ag NWs are 45.05 nm (±10.67 nm) and 15.93μm (±2.43 μm), respectively. The measured geometrical fill factor (FF) of the buried Ag NWs on the surface of PDMS substrate is 23.39%. As the figure shows, Ag NWs are well connected with each other forming a percolation network. After the electrodeposition of the Ni thin film on the exposed areas of the Ag NW network film for various periods, different morphologies of the Ni nanostructures were observed on the surface of the Ag NW network film, as shown in Figure 2b–e. **Table 1** illustrates the measured diameters of Ni coated Ag NWs for different electrodeposition periods of 5, 20, 50, and 100 s. Hereafter, sample A, B, C and D refer to the Ag NWs coated with Ni for 5, 20, 50, and 100 s of electrodeposition, respectively. The electrodeposition rates of the Ni layer on the Ag NW network film are calculated as 0.84 nm/s, 1.36 nm/s, 2.20 nm/s, and 2.33 nm/s for the samples A, B, C, and D, respectively. The increase of deposition rate is presumably due to the increase of surface area and electrical current for the electrochemical reaction. After a short Ni electrodeposition period (≈5 s), it was difficult to visually observe the formation of the Ni layer on the surface of the Ag NW network film (see Figure 2b). However, we could estimate the deposited thickness of the Ni layer (2.62 nm) from the electrical charge (≈0.0046 C, Figure S2, Supporting Information) by the electrodeposition process according to Faraday's law.[27] After 20 s of electrodeposition, discrete Ni nano-dot layers could be observed on the surface of Ag



small 2014,
DOI: 10.1002/smll.201400992

NANO MICRO small

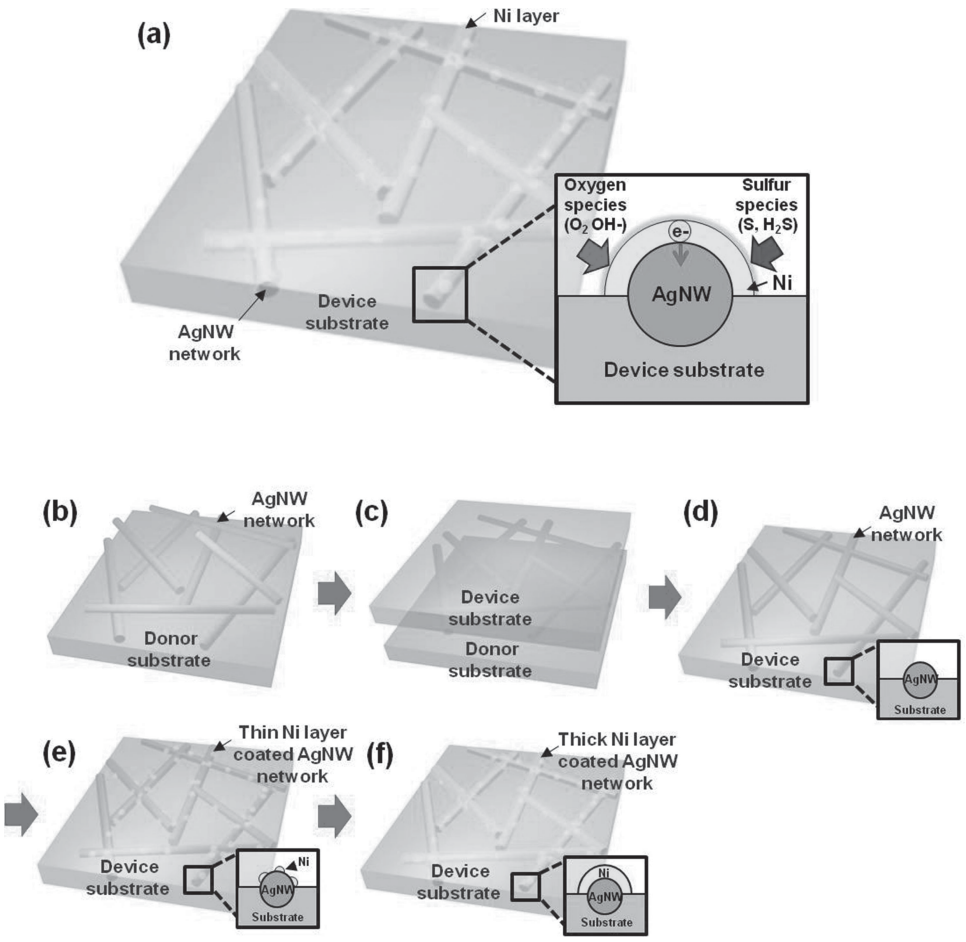


**Figure 1.** Mechanism and fabrication process: a) illustration of the Ni coated Ag NW network film, (inset) schematic of anti-oxidation and anti-sulfurization mechanisms of the Ni layer on the surface of Ag NW network; b–f) fabrication process for the Ni coated Ag NW network film b) formation of the Ag NW network on donor substrate by spray coating, c) formation of buried Ag NW network film on the device substrate (here, uncured PDMS film is poured and thermally cured), d) the Ag NW network film partially embedded on the surface of device substrate, e) nucleation of the thin Ni layer on the Ag NW network film by electrodepositionm, and f) formation of the thick Ni layer by longer electrodeposition on the Ag NW network film.

NWs (Figure 2c). After the electrodeposition for 50 and 100 s, the deposition of dense Ni layers could be observed on the surface of Ag NWs (Figure 2d,e). According to the electrical current-deposition time (*i–t*) curve of the samples, almost equal currents are measured for different samples at the same electrodeposition time, which verifies the repeatability of Ni electrodeposition process with similar exposed area of the Ag NW network film (Figure S1, Supporting Information). Therefore, we can assume that the thickness of the deposited Ni layer can be controlled by the electrodeposition periods.[27] The deposition thickness and shape of Ni layer can be also predicted by numerical simulation based on Faraday's law and Butler-Volmer equation (see Supporting Information for details).[27] Figure 2f shows a good agreement between simulated and measured diameters of Ag@Ni core–shell NWs for different electrodeposition periods. Figure 2g–i illustrate the evolution of the Ni layer thickness and current density at different electrodeposition periods ($t = 0, 20$ and 100 s) for half-embedded Ag NW. The thickness of Ni layer gradually increases with longer electrodeposition periods. Also, the thickness of Ni layer is almost equal in all angular orientations due to the uniform distribution of electrolytic potential and current density (e.g., –0.2021 V and 2.321 mA/m$^2$ at 20 s) around the Ag NW. Similar tendency is found in the case of the Ni electrodeposition on the protruded Ag NW (i.e., 5.21 area% embedded in the substrate) (Figure S1, Supporting Information) Therefore, the thickness and directional uniformity of the Ni coated layer can be easily controlled by the electrodeposition process.

The sheet resistances of the Ni coated Ag NW network films are lower than that of the pristine Ag NW network film. The high electrical resistance of Ag NW network film is caused by high junction resistance between Ag NWs.[6] The sheet resistance of the Ni coated Ag NW network film is gradually decreased by the increase of the Ni electrodeposition period (**Figure 3**a). For example, the Ni deposited Ag NW network films after a long electrodeposition period (i.e., 100 s) possesses a very low sheet resistance (9.92 (±5.42) Ω/sq) as compared with that of the pristine Ag NW network film (31.07(±3.56) Ω/sq). Increase of the conductivity could be due to the additional contribution of the outer Ni shell layer to the electrical conductance as well as bonding improvement between Ag NWs via welding effect at the NW junctions. As shown in Figure 2, the FF of Ag NW is increased by electrodeposited Ni layer


DOI: 10.1002/smll.201400992

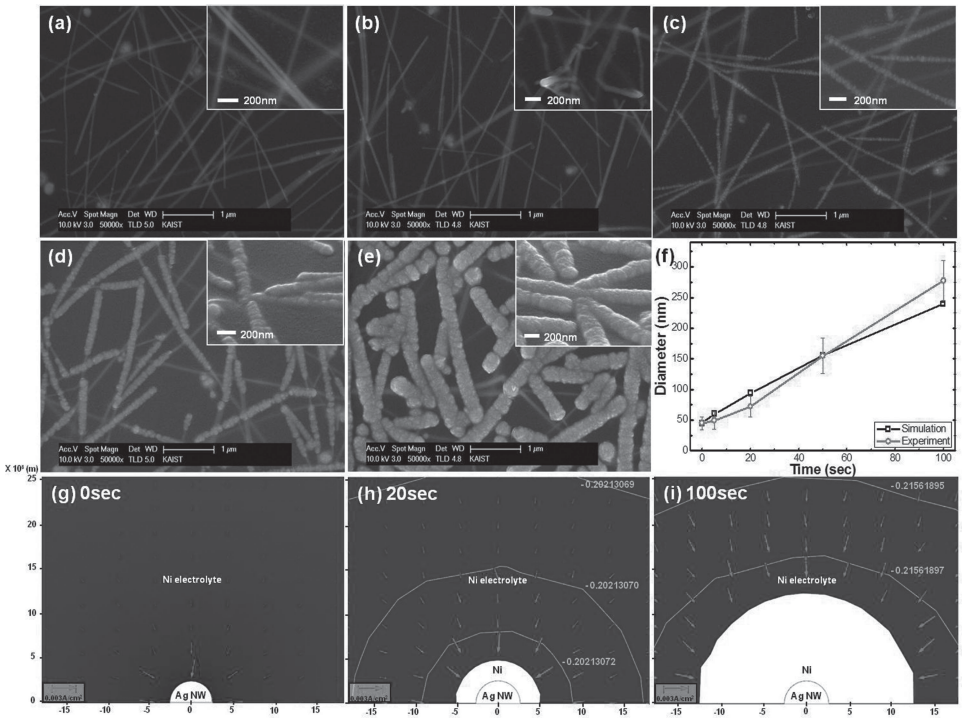


**Figure 2.** The surface SEM images of the Ag NW network film: a) pristine Ag NWs, b) sample A, c) B, d) C, and e) D; Ag NWs coated with Ni layer for various electrodeposition periods (0 s (a), 5 s (b), 20 s (c), 50 s (d) and 100 s (e)); f) measured and simulated diameters of Ag@Ni core–shell NWs; g–i) cross-sectional image of single Ag@Ni core–shell NW after different electrodeposition periods (g–i: 0, 20, and 100 s) obtained by numerical simulation. In this case, Ag NW was embedded in the substrate by 50% in area.

(23.39, 23.99, 29.34, 34.16, and 66.32% for pristine Ag NW, sample A, B, C, and D, respectively) which represents enlargement of the current-carrying area. It should be noted that the Ni shell layer was not electrodeposited onto some Ag NWs that were fully embedded into the substrate or electrically disconnected from percolation network. However, the electrodeposited Ni layer provided welding between loosely connected or separated Ag NWs as shown Figure 2d,e.

The transmittance spectra of the pristine Ag NW network film and Ni coated Ag NW network film were measured to quantify their optical characteristics. In order to quantify their transmittance without the substrate effect, we eliminated the background signals from the PDMS substrates (thickness ≈ 4 mm) by subtracting the absorbance of the PDMS substrate. Figure panels 3b and c illustrate the transmittance spectra and the transmittance at $\lambda$ = 550 nm for the pristine Ag NW network film and Ni coated Ag NW network film, respectively. At $\lambda$ = 550 nm, the transmittance of the pristine Ag NW network film is 85.2% but it gradually decreases to lower transmittance by longer period of Ni electrodeposition. ($T_{\lambda\ =\ 550\ \mathrm{nm}}$ = 81.41, 74.99, 48.66, and 37.01% for samples A, B, C, and D) This is due to the increase of FF of the Ag NW network film by the deposition of thicker Ni layers on the surface of Ag NWs.

The figure of merits (FoM) of TCEs, defined as the ratio of the electrical conductance and the optical conductance ($\sigma_{opt}/\sigma_{dc}$) is calculated by commonly used equation as follows:[28,29]

$$T = \left(1 + \frac{188.5}{R_s}\frac{\sigma_{opt}}{\sigma_{dc}}\right)^{-2}$$

where $R_s$ is the sheet resistance and $T$ is the transmission at 550 nm, respectively. The FoM of the pristine Ag NW network film is 72.62, while those of samples A, B, C, and D are 60.04, 46.79, 20.62, and 29.51, respectively (Figure 3d). The decrease of FoMs for the Ni coated Ag NW network is mainly due to the reduced transmittance. Furthermore, the

**Table 1.** Physical parameter changes of the Ag NW network film by the electrodeposition of Ni layer: average diameter, fill factor (FF), transmittance at 550 nm wavelength, and the sheet resistance.

| Sample name | Pristine Ag NW network film | A | B | C | D |
|---|---|---|---|---|---|
| Period of Ni electrodeposition [s] | 0 | 5 | 20 | 50 | 100 |
| Diameter [nm] | 45.05 (±10.67) | 49.23 (±14.33) | 72.33 (±17.12) | 154.85 (±29.14) | 277.60 (±32.88) |
| FF [%] | 23.39 | 23.99 | 29.34 | 34.16 | 66.32 |
| $T_{550nm}$ [%] | 85.27 | 81.41 | 74.99 | 48.66 | 37.01 |
| $R_s$ [Ω/sq] | 31.07 (±3.56) | 28.98 (±7.74) | 26.03 (±7.92) | 21.09 (±5.88) | 9.92 (±5.42) |



small 2014,
DOI: 10.1002/smll.201400992

NANO MICRO small

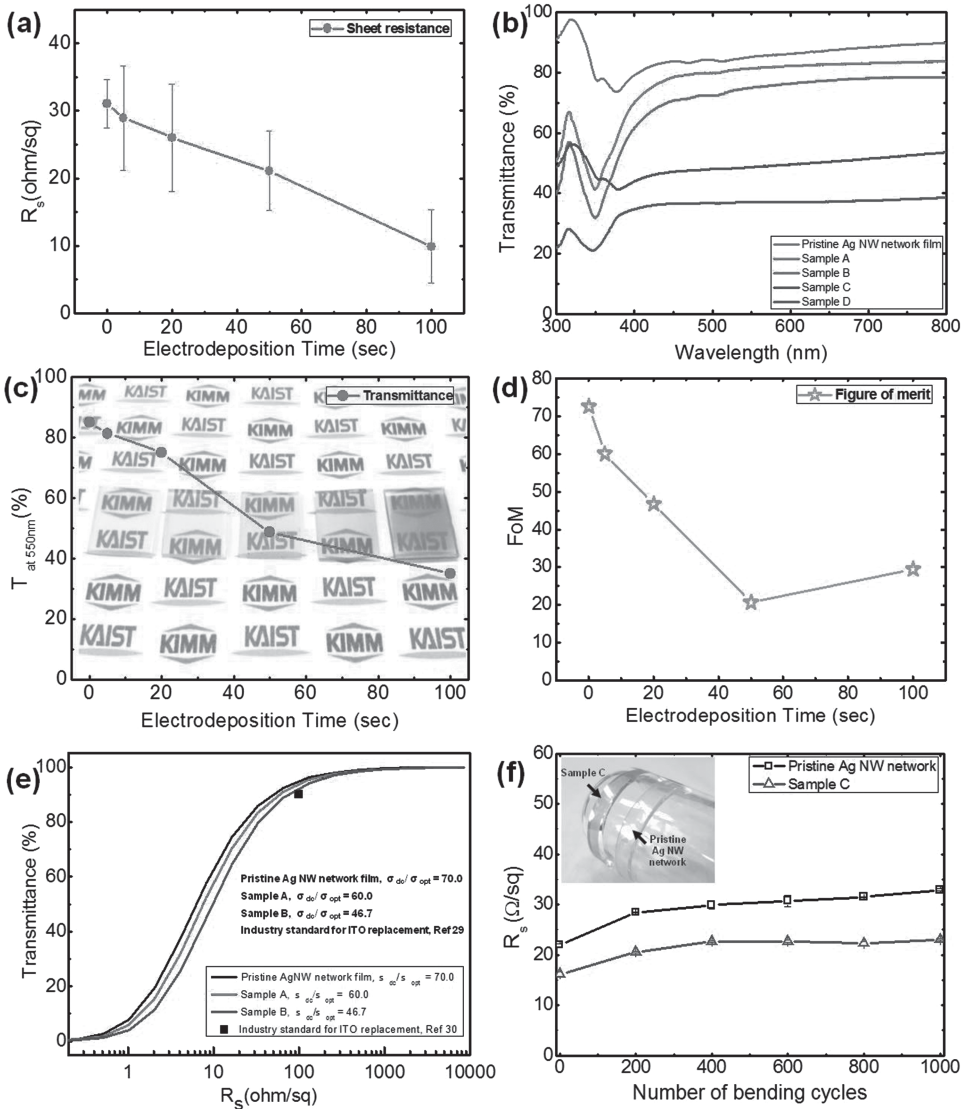


**Figure 3.** Physical parameter changes of the Ag NW network film by the electrodeposition of Ni layer: a) sheet resistance, b) transmittance spectra, and c) transmittance at $\lambda = 550$ nm, d) figure of merit (FoM), and e) transmittance vs sheet resistance plot of Ag NWs embedded on PDMS, Ni-coated Ag NW network films (5, 20 s), and the minimum industrial standard opto-electrical performance as an ITO replacement (black square). f) Sheet resistance changes for the pristine Ag NW network and Sample C under cyclic bending/relaxation.

FoM of the Ni coated Ag NW network film with short deposition periods (5 and 20 s) meet the minimum requirement of the industrial standard for ITO replacement as a transparent conductive electrode (FoM > 36) suggested in the previous report.[30] However, samples C and D show lower values than this criterion. The mechanical robustness is also an important factor for flexible and wearable electronic applications. To this end, we have conducted the bending test for more than 1000 bending/relaxation cycles from a flat ($\rho = \infty$) to bended ($\rho = 1$ cm) state. As shown in Figure 3f, the sheet resistances of the pristine Ag NW network and sample C are slightly increased from 21.98 Ω/sq and 16.16 Ω/sq to 32.92 Ω/sq and 23.04 Ω/sq, respectively, by 1000 cycles of bending but show gradual saturation. This result verifying that the Ni coated Ag NW network partially embedded on the substrate can be used as mechanically robust transparent conductive electrodes for flexible electronic applications.

The formation of the core–shell structure of Ag NW and Ni shell layer enables protection of the core Ag NWs from oxidative or corrosive environments. This could be confirmed by the measurement of sheet resistance of the samples and X-ray photoelectron spectroscopy (XPS) analysis before and after exposure to the chemically harsh environment (see **Figure 4**,**6** for the electrical measurement, and **Figure 5**, **7** for the XPS analysis). To evaluate the corrosion resistance of the Ni coated Ag NW networks in the air, the change of electrical resistance was measured under accelerated test (80 °C and 85% of relative humidity (RH)). Figure 4a,b show the changes of the sheet resistance of the pristine Ag NW network film and Ni coated Ag NW network film during the 80°C/85% RH accelerated test. After 12 h of 80 °C/85% RH accelerated test, the sheet resistance of the pristine Ag NW network film rapidly increased to 7.11 times ($R_s = 36.16$ Ω/sq to $R_s = 256.93$ Ω/sq). On the other hand, the sheet resistances


DOI: 10.1002/smll.201400992

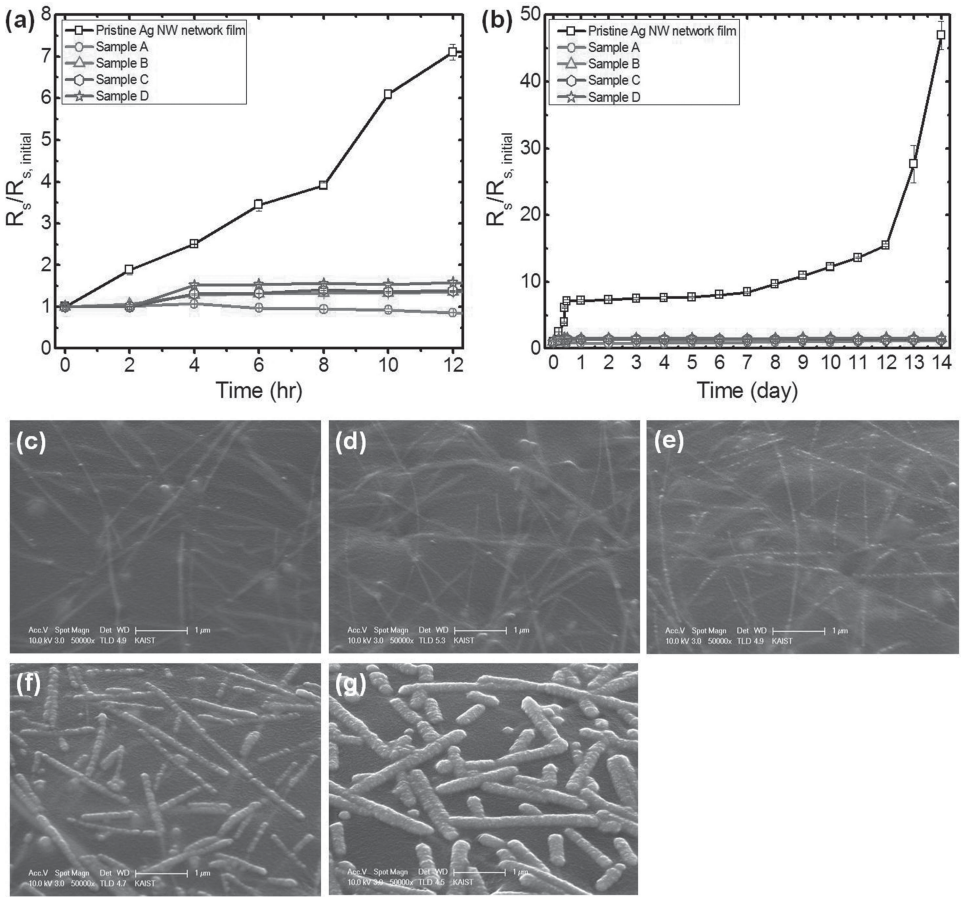


**Figure 4.** UV–Vis absorption measurement in transverse magnetic (TM) mode of fabricated nanostructure arrays: a) A0 NW array, A45 NW array, and A60 NW array; b) A0/gel NW array, A45/gel NW array, A60/gel NW array, Black dotted lines for each sub-figure represent non-polarized absorption of a) Ag thin film and b) Ag/gel-$TiO_2$ dual layer thin film, respectively.

of the samples A, B, C, and D were slightly changed to 0.89, 1.35, 1.38, and 1.58 times, respectively. Furthermore, we conducted the 80 °C/85% RH accelerated test for much longer periods. The sheet resistance of the pristine Ag NW network film was increased to 7.17 times after 1 day, which continued to grow up to 15.46 times within 12 days. However, it started to grow rapidly after 12 days, showing a dramatic raise up to 27.63 times and 46.96 times after 13 and 14 days, respectively. On the contrary, the sheet resistances of samples A, B, C, and D were only slightly increased to 1.18, 1.48, 1.37, and 1.54 times, respectively, after 14 days of 80°C/85% RH accelerated test.

The surface morphologies of the pristine and Ni coated Ag NW network films after 80°C/85% RH accelerated test were observed by scanning electron microscopy (SEM) analysis. For all the samples, there are no significant changes on the morphology of the Ag NW network films (compare Figure 2a–e with Figure 4c–g). However, the XPS results verify the change of material composition via chemical reaction. In Figure 5, the XPS spectra of the pristine Ag NW network film (Figure 5a–c) and sample C (Figure 5d–g) before and after the 80 °C/85% RH accelerated test are shown. The peak positions of the Ag $3d_{3/2}$ and Ag $3d_{5/2}$ shifted from 374.23 eV to 374.70 eV and from 368.19 to 368.67 eV, respectively, after 80 °C/85% RH accelerated test for the pristine Ag NW network film (Figure 5a). Here, the increase of binding energy mainly stems from the sulfurization of Ag.[19] In addition, the sulfur (S) 2p peaks were observed after 80 °C/85% RH accelerated test (Figure 5b). The sulfurization of Ag NW is caused by sulfur-containing gases such as carbonyl sulfide (OCS), sulfur dioxide ($SO_2$) and carbon disulfide ($CS_2$), which is enhanced at higher relative humidity.[31–33] The O 1s peak for pristine Ag NW at 532.66 eV was observed, which shows similar value with those of PDMS in the literature.[34] This broad O 1s peak is attributed by interaction between oxygen in the carboxyl group of the PVP chain on surface of the Ag NWs[19,35] (Figure 5c). In contrast, the changes of Ag 3d peak positions (368.17 eV to 368.40 eV for Ag $3d_{3/2}$ and 374.14 to 374.38 eV for Ag $3d_{5/2}$) for the sample C are smaller than those for the pristine Ag NW network film, which confirms better resistance against sulfurization by the Ni layer electroplated on the Ag NWs. Moreover, the sample C shows little changes of Ni peaks (Figure 5g) after the 80 °C/85% RH accelerated test. According to our XPS spectra measurements, the Ag NW network film coated with the Ni layer is less sulfurized than the pristine Ag NW network after the 80 °C/85% RH accelerated test. For the Ag NW network film coated with the Ni layer for short periods (5–20 s), NWs are only partially covered with Ni layer and considerable portion of Ag NWs are exposed to the environment. In this case, the



small 2014,
DOI: 10.1002/smll.201400992

NANO MICRO small

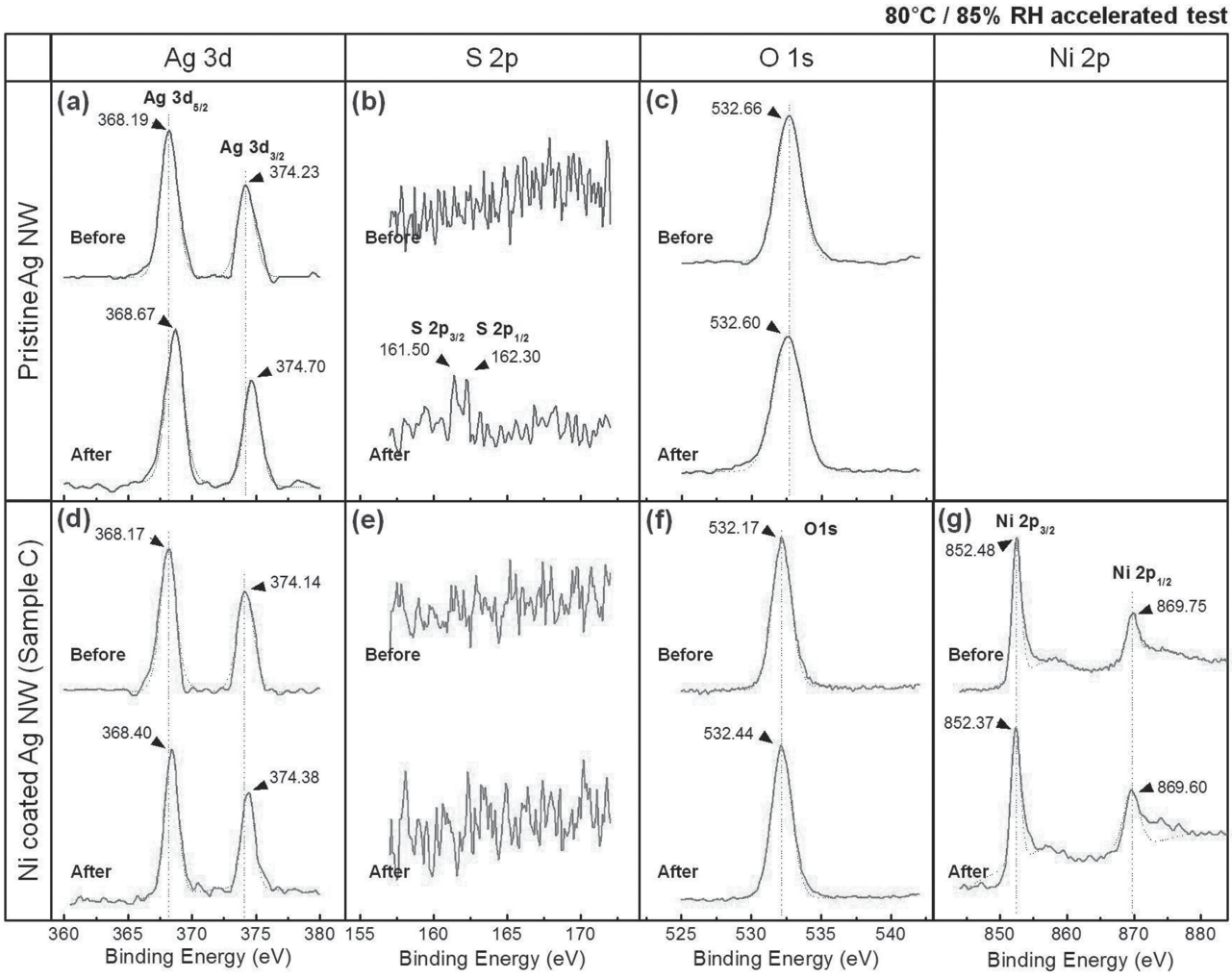


**Figure 5.** Change of XPS spectra for the pristine Ag NW network film and sample C by 80 °C/85% RH accelerated test: a) Ag 3d spectra, b) S 2p spectra, c) O 1s spectra of the pristine Ag NW network film before and after 80 °C/85% RH accelerated test; d) Ag 3d spectra, e) S 2p spectra, f) O 1s spectra, and g) Ni 2p spectra of the sample C before and after 80 °C/85% RH accelerated test.

anti-sulfurization effect of the Ni layer could be explained by reactive series of metals[36] and galvanic corrosion.[37] During the exposure, the coated Ni film and Ag NWs act as cathode and anode in the galvanic cell, respectively, since the standard electromotive force of Ni ($V_{sce}$ = –0.799 V) is much lower than that of Ag ($V_{sce}$ = 0.257 V). When both materials are exposed to corrosive environment, the cathodic protection layer (Ni) donates electrons to Ag NWs so that it prevents the corrosion of Ag NWs. On the other hand, after electrodeposition for longer periods (50–100 s, sample C and D), Ag NWs are fully covered with a Ni shell layer. In this case, the Ni shell forbids Ag NWs from a direct contact to sulfur. Therefore, in this case, physical barrier against the sulfurization reaction and diffusion by the Ni layer as well as its electron donation prohibit the sulfurization of the Ag NW network film and prevent the decrease of electrical conductance.

The chemical stability of the Ni coated Ag NW network film against sulfurization and oxidation was characterized by measuring the electrical resistance of the samples during $Na_2S$ solution exposure (i.e. 5 wt% of $Na_2S$ in DI water). Figure 6a presents the changes of the sheet resistance for the pristine and Ni coated Ag NW network films after the immersion in $Na_2S$ solution. The sheet resistance of the pristine Ag NW network film is drastically increased by 113.83 times (15.90 Ω/sq to 1810.00 Ω/sq) only after 21 s. The sample A and B also exhibit a rapid corrosion by $Na_2S$ solution with a dramatic increase of the electrical resistance. However, the sample C and D present a tremendous enhancement of chemical resistance against corrosion, which is verified by much smaller changes of electrical resistances (i.e., 6.44 and 8.48 times increase of the sheet resistance for the samples C and D after 300 s in the $Na_2S$ solution). As shown in Figure 6b, the pristine Ag NWs are broken into small pieces due to the corrosion. Thin Ni layers on the Ag NWs could not protect them from sulfurization and oxidation reaction as shown in Figure panels 6c-d for the samples A and B. However, the samples C and D exhibit the preservation of structural integrity without any fracture or damage on the surface (Figure 6e,f). After the sulfurization reaction, a few cubic crystallites of $Ag_2S$ are observed on the Ag NW network film (Figure 6f). The XPS results for the pristine Ag NW network film before and after the reaction with the $Na_2S$ solution are shown in Figure 7a–c. When Ag NW reacted with $Na_2S$ solution, wider spectrum of Ag 3d, O1s with several small peaks and


DOI: 10.1002/smll.201400992

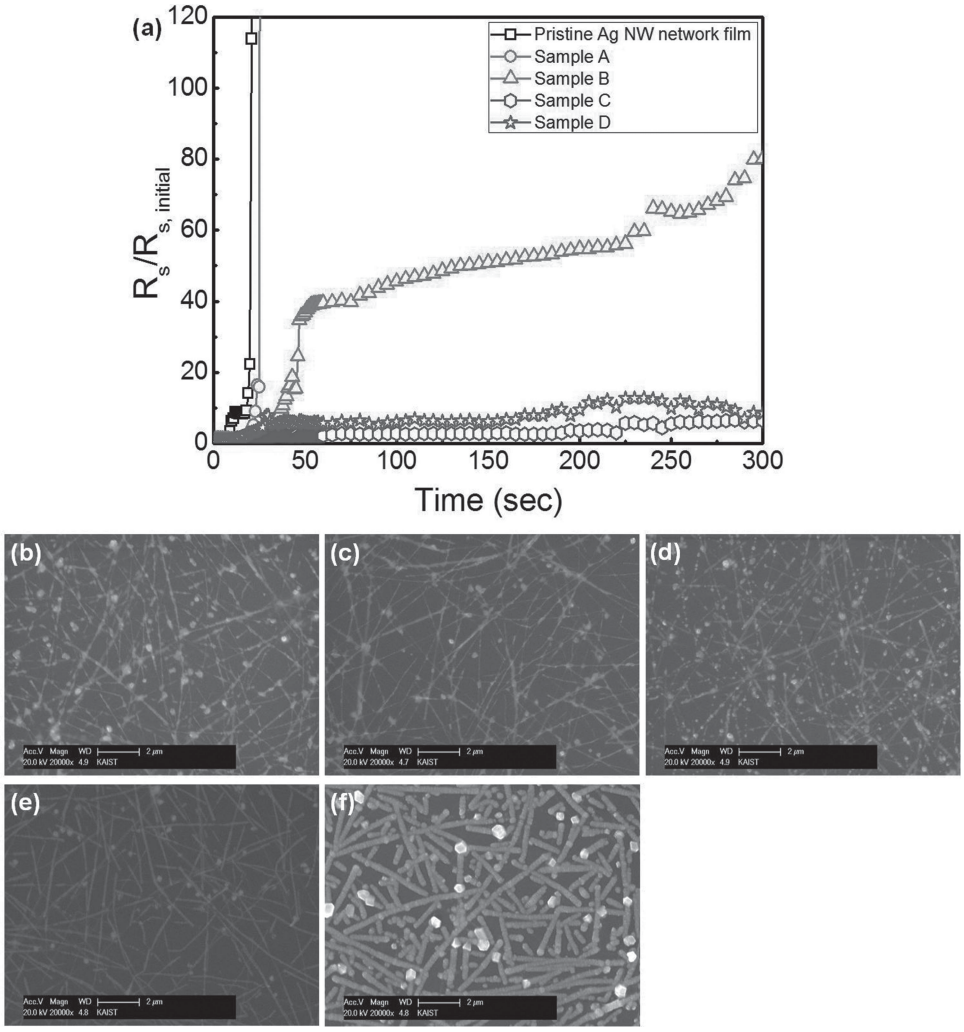


**Figure 6.** Effect of the Ni coating on the corrosion resistance of the Ag NW network film in $Na_2S$ liquid-phase corrosion test: a) Sheet resistance changes for the pristine and Ni coated Ag NW network film by exposure to the $Na_2S$ solution for 300 s. SEM images of the b) pristine Ag NW network film and samples c) A, d) B, e) C, and f) D after immersing into the $Na_2S$ solution for 300 s.

S 2p peaks were observed (Figure 7a–c). Here, the wide Ag 3d spectrum can be deconvoluted into the six peaks ($E_B$ = 369.30 eV, 364.90 eV and 368.11 eV for Ag $3d_{5/2}$ and $E_B$ = 375.40 eV, 374.32eV and 373.00 eV for Ag $3d_{3/2}$) as shown in Figure 7a. $E_B$ = 369.30 eV (Ag $3d_{5/2}$) and $E_B$ = 375.40 eV (Ag $3d_{3/2}$) of sample C are higher than those of the pristine Ag NW (368.19 eV and 374.23 eV for Ag $3d_{5/2}$ and Ag $3d_{3/2}$, respectively) due to the sulfurization of Ag NW by $H_2S$ existing in the $Na_2S$ solution.[19] The lower binding energies $E_B$ = 364.90eV and 368.11eV (Ag $3d_{5/2}$) and $E_B$ = 373.00eV and 374.32 eV (Ag $3d_{3/2}$) indicate the formation of $Ag_2O$ by the absorption and reaction with oxygen species such as $OH^-$ ion[38] and $O_2$[39] within the $Na_2S$ solution. The oxidation of Ag can also be confirmed by the deconvoluted lower peaks at 529.40 eV and 530.70 eV for O1s (Figure 7c).[40,41] In contrast, the sample C presents much smaller change of the peak positions of Ag $3d_{3/2}$ due to much less formation of $Ag_2S$ in the sample C than in the pristine Ag NW (Figure 7d). The peak position of Ni $2p_{3/2}$ is slightly shifted due to small sulfurization of Ni shell. Higher satellite peaks at 855.50 eV for Ni $2p_{3/2}$ and 872.90 eV for Ni $2p_{5/2}$ are caused by the oxidation of Ni[42] with oxygen species in the $Na_2S$ solution. In summary, we can confirm that Ag NW network film is protected from the severe sulfurization and oxidation by the Ni shell layer in spite of its minor corrosion.

The anti-corrosion mechanism of Ag NWs by the thick Ni shell layer (samples C and D) can be explained by the galvanic corrosion and thermodynamic effect. The electrode potential difference of Ni and Ag induces cathodic protection of Ag NWs by the Ni shell layer, resulting in the delay of galvanic corrosion such as oxidation and sulfurization of Ag NWs. In addition, the Ni shell layer can reduce the sulfurization of the core Ag NW structure due to the resistance of Ni against the sulfurization reaction. The Gibbs free energy (ΔG) for the formation of nickel sulfide (NiS) in $Na_2S$ aqueous solution at room temperature is –119.7 kJ/mol, which is smaller than that value of silver sulfide ($Ag_2S$), –280.7 kJ/mol.[43] Therefore, the sulfurization of Ni shell layer is much slower than that of the core Ag NWs. As a result, Ag NWs can be protected from the rapid sulfurization via the barrier effect of the Ni shell layer.

We further illustrate the sulfurization and oxidation effects of the pristine Ag NW network film and sample C



small 2014,
DOI: 10.1002/smll.201400992

NANO MICRO small

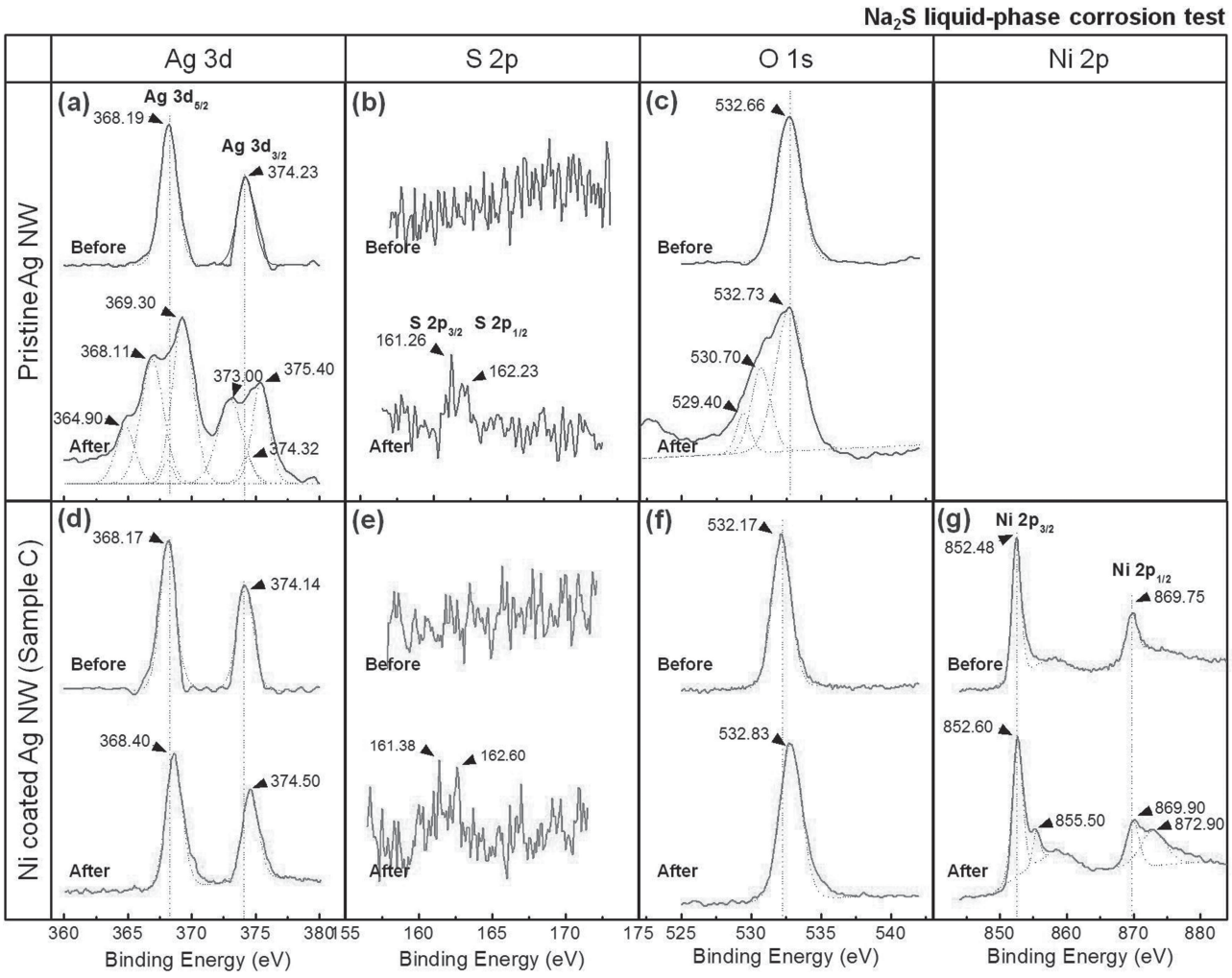


**Figure 7.** Change of XPS spectra for the pristine Ag NW network film and sample C by $Na_2S$ liquid-phase corrosion test: a) Ag 3d spectra, b) S 2p spectra, c) O 1s spectra of the pristine Ag NW network film before and after $Na_2S$ liquid-phase corrosion test; d) Ag 3d spectrum, e) S 2p spectrum, f) O 1s spectrum, and g) Ni 2p spectrum of the sample C before and after $Na_2S$ liquid-phase corrosion test.

by constructing a simple LED circuit (**Figure 8**a). Here the pristine and Ni coated Ag NW network films were used as a conductor serially connected to the LED lamp. As depicted in Figure 8b–d, the LED was turned off since the electrical conductance of the pristine Ag NW network film was electrically nonconductive after 80 °C/85% RH accelerated test and $Na_2S$ liquid-phase corrosion test. On the other hand, the illumination intensity of LED lamp was not significantly degraded for sample C after 80 °C/85% RH accelerated test and $Na_2S$ liquid-phase corrosion test (Figure 8e–g). This result confirms that Ni coating on the Ag NW network maintains the functionality of the interconnection in the circuit.

## 3. Conclusion

In summary, we have developed a novel method to improve the chemical stability of the Ag NW network film based transparent conductive electrode simply by local electrodeposition of Ni layer along the Ag NWs. We observed enhancement of the electrical conductivity after electrodeposition of Ni layer on the Ag NW network film by the welding effect. Furthermore, Ni coated Ag NW network films exhibit an excellent chemical resistance against the oxidation as well as the sulfurization reaction compared with very large resistance deviation of the pristine Ag NW network exposed to the harsh environment. Cathodic protection and chemical resistance of Ni shell layer prevent the oxidation and sulfurization of the core Ag NWs. Therefore, this method can maintain the performance of devices without degradation. We believe that our proposed method can be applicable to the chemical protection of a variety of conductive nanomaterial based electrodes. Especially, this method will be extremely useful for the applications in which conductive nanomaterial electrodes are directly exposed to the harsh environment or immersed in chemically reactive liquids. Moreover, the applications can be further extended to toxic chemical sensing in harsh environment.

## 4. Experimental Section

Ag NWs were synthesized by the polyol method according to the literature.[14] First, 5.86 g of polyvinylpyrrolidone (PVP) in 190 mL of glycerol was heated at 55 °C. Then, 0.059 g of NaCl, 0.5 mL of DI water and 1.58 g of $AgNO_3$ were poured into the preheated


DOI: 10.1002/smll.201400992

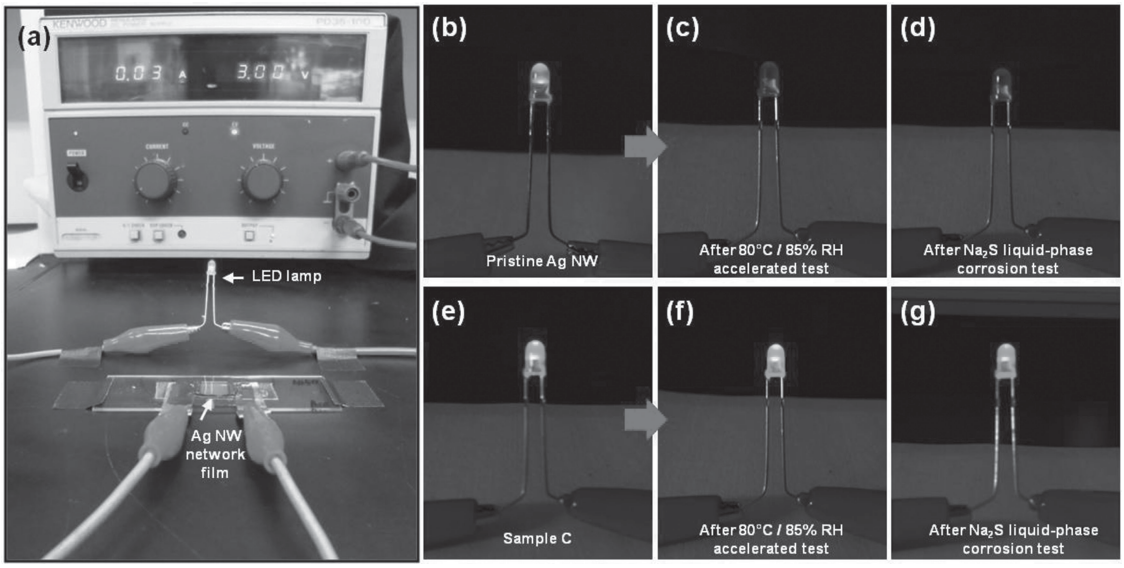


**Figure 8.** Corrosion effect of the Ag NW network based interconductor in the electrical circuit: a) Photograph of the electrical circuit; LED is connected to the power source via Ag NW network based conductor. Illumination of LED connected via a pristine Ag NW network film b) before, c) after 80 °C/85% RH accelerated test, and d) after $Na_2S$ liquid-phase corrosion test. Photograph of LED lamp using sample C as a connector; e) before, f) after 80 °C/85% RH accelerated test and g) after $Na_2S$ liquid-phase corrosion test.

mixture. The solution was heated up to 155 °C within 10 min with gentle stirring. Finally, the solution was filtered by vacuum filtration method and Ag NWs were stored in diluted methanol for further experiments. Ni layer was electrodeposited on the exposed surface of the Ag NW network film. Here, a Ni electrodeposition watt bath consisting of 1 m nickel sulfate hexahydrate ($NiSO_4 \cdot 6H_2O$), 0.2 m nickel chloride hexahydrate ($NiCl_2 \cdot 6H_2O$) and 0.5M boric acid ($H_3BO_3$) in DI water was used. A three electrode cell configuration including Ag NW network film buried on the PDMS film as a working electrode, platinum (Pt) coated titanium (Ti) plate as an insoluble counter electrode, and Ag/AgCl (saturated KCl) electrode as a reference electrode was used at a room temperature condition with a stirring rate of 200 rpm. The Ag NW network film buried on the surface of PDMS was electrically connected with aluminum plate by painting the silver paste at the edge of Ag NW network film and passivated by painting a commercial manicure except the working area (exposed area = 15 mm × 15 mm) for electrodeposition. A constant potential of −0.9 V was applied for various electrodeposition periods (0–100 s) by using a potentiostat/galvanostat (601D, CH Instruments, Inc.). The surface morphologies of the samples were investigated by using a scanning electron microscope (SEM, Sirion FE-SEM, FEI) and composition of the samples were determined by energy dispersive spectroscopy (EDS). Also, the chemical compositions and crystallographic structures of the Ag NW network and Ni coated Ag NW network were studied by XPS (Sigma Probe, Thermo VG Scientific, Inc.) and X-ray diffraction (Rigaku D/max-2500) using a Cu K$\alpha$ radiation ($\lambda = 1.5405$ Å) at 40 kV and 300 mA.

## Supporting Information

*Supporting Information is available from the Wiley Online Library or from the author.*

## Acknowledgements

*This research was supported by the grants from the Basic Science Research Program (2013006809) and Global Frontier R&D Program (2011–0031563) funded by the National Research Foundation (NRF) and from KIMM (Korea Institute of Machinery & Materials) Research (SC0940) under the Ministry of Science, ICT and Future Planning of Korea. This work was also financially supported by the Graphene Materials and Components Development Program of MOTIE/KEIT (10044412).*

[1] H. Schmidt, H. Flugge, T. Winkler, T. Bulow, T. Riedl, W. Kowalsky, *Appl. Phys. Lett.* **2009**, *94*.
[2] J. P. B. Mark, J. Pellerite, M. A. Boulos, P. M. Campbell, A. J. H. Eileen, M. Haus, M. Nirmal, M. D. Radcliffe, R. R. Roberts, J. K. W. John, J. Stradinger, B. T. Weber, In 14.2: New Transparent Electrodes for Cholesteric Liquid Crystal Displays, SID Symposium Digest of Technical Papers, SID Symposium Digest of Technical Papers, New York **2012**, *172*.
[3] S.-Y. R. K. H. Lee, J. H. Kwon, S. W. Kim, H. K. Chung, In 9.3: 2.2" QCIF Full Color Transparent AMOLED Display, SID Symposium Digest of Technical Papers, New York **2012**.
[4] D. S. Hecht, L. B. Hu, G. Irvin, *Adv. Mater.* **2011**, *23*, 1482.
[5] C. Peng, Z. Jia, H. Neilson, T. Li, J. Lou, *Adv. Eng. Mater.* **2013**, *15*, 250.
[6] L. B. Hu, H. S. Kim, J. Y. Lee, P. Peumans, Y. Cui, *ACS Nano* **2010**, *4*, 2955.
[7] S. Kim, J. Yim, X. Wang, D. D. C. Bradley, S. Lee, J. C. Demello, *Adv. Funct. Mater.* **2010**, *20*, 2310.
[8] S. Bae, H. Kim, Y. Lee, X. F. Xu, J. S. Park, Y. Zheng, J. Balakrishnan, T. Lei, H. R. Kim, Y. I. Song, Y. J. Kim, K. S. Kim, B. Ozyilmaz, J. H. Ahn, B. H. Hong, S. Iijima, *Nat. Nanotechnol.* **2010**, *5*, 574.
[9] C. Celle, C. Mayousse, E. Moreau, H. Basti, A. Carella, J. P. Simonato, *Nano Res.* **2012**, *5*, 427.
[10] C. H. Liu, X. Yu, *Nanoscale Res. Lett.* **2011**, *6*.
[11] Y. G. Sun, Y. N. Xia, *Adv. Mater.* **2002**, *14*, 833.




DOI: 10.1002/smll.201400992

[12] K. E. Korte, S. E. Skrabalak, Y. N. Xia, *J. Mater. Chem.* **2008**, *18*, 437.
[13] Y. G. Sun, B. Mayers, T. Herricks, Y. N. Xia, *Nano Lett.* **2003**, *3*, 955.
[14] J. Lee, I. Lee, T. S. Kim, J. Y. Lee, *Small* **2013**, *9*, 2887.
[15] C. H. Chung, T. B. Song, B. Bob, R. Zhu, Y. Yang, *Nano Res.* **2012**, *5*, 805.
[16] V. Scardaci, R. Coull, P. E. Lyons, D. Rickard, J. N. Coleman, *Small* **2011**, *7*, 2621.
[17] D. Kim, L. J. Zhu, D. J. Jeong, K. Chun, Y. Y. Bang, S. R. Kim, J. H. Kim, S. K. Oh, *Carbon* **2013**, *63*, 530.
[18] H. H. Khaligh, I. A. Goldthorpe, *Nanoscale Res. Lett.* **2013**, *8*.
[19] J. L. Elechiguerra, L. Larios-Lopez, C. Liu, D. Garcia-Gutierrez, A. Camacho-Bragado, M. J. Yacaman, *Chem. Mater.* **2005**, *17*, 6042.
[20] H. Aziz, Z. Popovic, C. P. Tripp, N. X. Hu, A. M. Hor, G. Xu, *Appl. Phys. Lett.* **1998**, *72*, 2642.
[21] J. A. C. Hillman, S. Binfield, In Silver and Sulfur: Case Studies, Physics, and Possible Solutions, SMTA International 2007 Edina, MN, *13*.
[22] A. K. N. Chawdhury, M. G. Harrison, D. H. Hwang, A. B. Holmes, R. H. Friend, *Synth. Metals* **1999**, *102*, 2.
[23] J. Liang, L. Li, K. Tong, Z. Ren, W. Hu, X. Niu, Y. Chen, Q. Pei, *ACS Nano* **2014**, *8*, 1590.
[24] X. Y. Zeng, Q. K. Zhang, R. M. Yu, C. Z. Lu, *Adv. Mater.* **2010**, *22*, 4484.
[25] A. R. Rathmell, M. Nguyen, M. F. Chi, B. J. Wiley, *Nano Lett.* **2012**, *12*, 3193.
[26] Y. Tao, Y. X. Tao, L. Y. Wang, B. B. Wang, Z. G. Yang, Y. L. Tai, *Nanoscale Res. Lett.* **2013**, *8*.
[27] M. Paunovic, M. Schlesinger, in *Fundamentals of Electrochemical Deposition*, 2nd ed., Wiley-Interscience, Hoboken, NJ **2006**, Ch. 11.
[28] S. De, T. M. Higgins, P. E. Lyons, E. M. Doherty, P. N. Nirmalraj, W. J. Blau, J. J. Boland, J. N. Coleman, *ACS Nano* **2009**, *3*, 1767.
[29] J. V. van de Groep, P. Spinelli, A. Polman, *Nano Lett* **2012**, *12*, 3138.
[30] S. De, J. N. Coleman, *ACS Nano* **2010**, *4*, 2713.
[31] R. L. P. H. E. Bennett, D. K. Burge, J. M. Bennett, *J. Appl. Phys.* **1969**, *40*, 11.
[32] T. E. Graedel, J. P. Franey, G. J. Gualtieri, G. W. Kammlott, D. L. Malm, *Corros. Sci.* **1985**, *25*, 1163.
[33] T. E. Graedel, *J. Electrochem. Soc.* **1992**, *139*, 1963.
[34] P. Holgerson, D. S. Sutherland, B. Kasemo, D. Chakarov, *Appl. Phys. A, Mater,* **2005**, *81*, 51.
[35] C. W. Xiao, H. T. Yang, C. M. Shen, Z. A. Li, H. R. Zhang, F. Liu, T. Z. Yang, S. T. Chen, H. J. Gao, *Chinese Phys.* **2005**, *14*, 2269.
[36] J. E. Brady, G. E. Humiston, in *General Chemistry, Principles and Structure*, 3rd ed., Wiley, New York **1982**.
[37] R. W. Revie, H. H. Uhlig, in *Uhlig's Corrosion Handbook*, 3rd ed., Wiley, Hoboken, N.J, **2011**.r
[38] X. Bao, M. Muhler, B. Pettinger, Y. Uchida, G. Lehmpfuhl, R. Schlogl, G. Ertl, *Catal. Lett.* **1995**, *32*, 171.
[39] J. Y. Liu, K. G. Pennell, R. H. Hurt, *Environ. Sci. Technol.* **2011**, *45*, 7345.
[40] E. R. Savinova, D. Zemlyanov, B. Pettinger, A. Scheybal, R. Schlogl, K. Doblhofer, *Electrochim. Acta* **2000**, *46*, 175.
[41] Y. Abe, T. Hasegawa, M. Kawamura, K. Sasaki, *Vacuum* **2004**, *76*, 1.
[42] D. L. Legrand, H. W. Nesbitt, G. M. Bancroft, *Am. Mineral* **1998**, *83*, 1256.
[43] P. Y. Fuxiang Huang, Y. Xu, Y. Zhang, *Adv. Mater. Res.* **2011**, *311*, 2132.

Received: April 10, 2014
Revised: May 28, 2014
Published online: